Received: 10 July 2019 | Revised: 18 December 2020 | Accepted: 22 December 2020

DOI: 10.1002/dep2.134

ORIGINAL RESEARCH ARTICLE

The Depositional Record Open Access
A journal of the International Association of Sedimentologists
WILEY

Calcium transfer and mass balance associated with soil carbonate in a semi-arid silicate watershed (North Cameroon): An overlooked geochemical cascade?

Fabienne Dietrich[1] | **Nathalie Diaz**[1,2] | **Pierre Deschamps**[3] | **David Sebag**[1,4,5] | **Eric P. Verrecchia**[1]

[1]Earth Surface Dynamics Institute, Lausanne University, Lausanne, Switzerland

[2]Department of Geography, Royal Holloway University of London, Engham, UK

[3]CNRS, INRA, Collège de France, CEREGE, Aix-Marseille University, Aix-en-Provence, France

[4]UNIROUEN, UNICAEN, CNRS, Normandie Université, Rouen, France

[5]IFP Energies Nouvelles (IFPEN), Rueil-Malmaison, France

Correspondence
Fabienne Dietrich, Earth Surface Dynamics Institute, Lausanne University, Lausanne, Switzerland.
Email: fabienne.dietrich@unil.ch

Funding information
Schweizerischer Nationalfonds zur Förderung der Wissenschaftlichen Forschung, Grant/Award Number: 200021-147038

Abstract

Calcium is a key element of the Earth system and closely coupled to the carbon cycle. Weathering of silicate releases Ca, which is exported and sequestered in oceans. However, pedogenic calcium carbonate constitutes a second Ca-trapping pathway that has received less attention. Large accumulations of pedogenic calcium carbonate nodules, associated with palaeo-Vertisols, are widespread in North Cameroon, despite a carbonate-free watershed. A previous study suggested that a significant proportion of Ca released during weathering was trapped in palaeo-Vertisols but the pathways involved in the transfer of Ca from sources (the granite and the Saharan dust) to a temporary sink (the carbonate nodules) remain unclear. This study aims to compare the distribution of elements in carbonate nodules and their associated past and present compartments for Ca in the landscape. These compartments are all characterised by a distinctive geochemical composition, resulting from specific processes. Three end members have been defined based on geochemical data: (a) the granite and its residual products, dominated by K_2O and Na_2O, Ti and Zr, HREE, and a positive Ce anomaly; (b) the soil parental material and the Saharan dust, dominated by Al_2O_3, Fe_2O_3 and MgO, V, HREE, and a positive Ce anomaly; and finally (c) the carbonate nodules, which are dominated by CaO, a depletion in V, Ti and Zr, and an enrichment in REE with a negative Ce anomaly. Mass balance calculations in soil profiles demonstrated that the accumulation of Ca in carbonate nodules exceeds the Ca released by chemical weathering of the parental material, because of a continuous accumulation and contribution from lateral transfers. Consequently, at the landscape scale, carbonate nodules associated with palaeo-Vertisols constitute a temporary sink for Ca. Such a spatial relationship between sources and transient compartments opens an avenue to the new concept of 'geochemical cascade', similar in terms of geochemistry, to the concept of 'sediment cascade' developed by continental sedimentologists.

KEYWORDS

calcium cycle, carbonate nodules, Chad Basin, geochemical cascade, palaeo-Vertisol, silicate watersheds

1 | INTRODUCTION

Calcium is the fifth most abundant element in the Earth's crust (Rudnick & Gao, 2003) and is coupled to the carbon cycle at two different time scales (Tipper et al., 2016): (a) in the short-term carbon cycle, Ca is an important micronutrient for all organisms, for example, to maintain cell wall stability (Da Silva & Williams, 2001), and (b) in the long-term carbon cycle, Ca released during silicate weathering and sequestered as marine carbonate regulates atmospheric CO_2 concentrations (Berner et al., 1983; Walker et al., 1981). Indeed, during silicate weathering, CO_2 is sequestered and Ca is released from Ca-bearing minerals, such as Ca-plagioclases for instance, following the equation below (Urey, 1952):

$$2CO_2 + 3H_2O + CaSiO_3 \rightarrow Ca^{2+} + 2HCO_3^- + Si(OH)_4 \quad (1)$$

The Ca^{2+} cation is then transported into rivers and transferred to the ocean in solution, where it is precipitated, mainly as marine carbonate. By assuming that the composition of the rivers is partly controlled by the watershed lithology, numerous studies indirectly quantify silicate weathering rates in order to estimate atmospheric/soil CO_2 consumption (Berner et al., 1983; Gaillardet et al., 1999; Garrels & Mackenzie, 1971; Holland, 1984; Meybeck, 1987; Négrel et al., 1993). Nonetheless, an alternative pathway may exist for Ca: it can be sequestered as pedogenic carbonate on continents, at least temporarily, and thus, a significant part of the Ca released from silicate weathering is not directly transferred into the rivers towards oceans. Few studies have pointed out the significance of secondary carbonate precipitation and the biases they may induce in calculating the fraction of riverine cations derived from carbonate and silicate sources, and the final silicate chemical weathering rate (Bickle et al., 2015; Jacobson et al., 2002; Tipper et al., 2006). Indeed, pedogenic carbonates have received little attention. Defined as secondary calcium carbonate precipitations inside soils (Lal et al., 2000; Verrecchia, 2011), pedogenic carbonates may act as a long-term sink regarding C and Ca (Monger et al., 2015) and are an important part of the soil inorganic C (Eswaran et al., 2000; Zamanian et al., 2016). The average residence time of soil inorganic C is estimated at least as millennia (Monger et al., 2015; Schlesinger, 1985). Moreover, processes leading to the formation of secondary calcium carbonate, for example, nodules, are still unclear (Zamanian et al., 2016), as well as their impact and role in the C and Ca coupled biogeochemical pathways and cycles.

In the Far North region of Cameroon, pedogenic carbonate nodules are widespread (Brabant & Gavaud, 1985; Diaz et al., 2016a; Dietrich et al., 2017; Martin, 1961; Morin, 2000; Sieffermann, 1967). Large accumulations of such nodules have been observed associated with palaeo-Vertisols inherited from the last humid period (Diaz et al., 2016a, 2018), that is, the African Humid Period, from 14.8 to 5.5 ka BP (de Menocal et al., 2000). These accumulations represent a large quantity of Ca, especially because they are found in a silicate watershed, which has a low overall Ca content.

In a previous study using Sr and Nd isotopes, Dietrich et al. (2017) identified one Ca source as a local plagioclase mixed with a lesser amount of Saharan dust. This mainly local contribution has not often been documented in other settings, except in similar palaeo-Vertisol environments (Durand et al., 2006; Violette et al., 2010a). Moreover, the causes and amplitudes of the sequestered Ca preservation in this type of terrestrial geosystem remain unclear (Dietrich et al., 2017).

As described in previous studies (Aide & Smith-Aide, 2003; Aubert et al., 2001; Braun et al., 1998; Compton et al., 2003; Laveuf & Cornu, 2009; Öhlander et al., 1996; Sako et al., 2009; Stiles et al., 2003), the distributions of major, trace and REE (i.e. Na, K, Rb, Mg, Ca, Sr, Ba, Y, Ti, Zr, V, Mn, Fe, Al, U, La, Ce, Pr, Nd, Sm, Eu, Gd, Tb, Dy, Ho, Er, Tm, Yb and Lu) were also used in the various compartments composing the landscape, to identify the pedogenic processes involved in the formation of these carbonate nodules. Coupled with mineralogical, carbonate content and cation exchange capacity (CEC) analyses, compartments of the past calcium cycle have been identified in the present-day landscape. Once, the compartments have been defined and reconstructed, a calcium mass balance can be calculated in order to assess the importance of carbonate nodule precipitation in the calcium cycle.

2 | GEOLOGICAL SETTING

The study site is located at the foot of Mandara Mountains (orientated in an SW–NE direction) in the Mayo Kaliao watershed (Diamaré piedmont, Figure 1A,B). This Mayo ('Mayo' in the local Fufulde language means 'intermittent stream') belongs to the endorheic Chad Basin, as it is a tributary of the Logone River, the second largest outflow of Lake Chad (Olivry & Naah, 1999). The mean annual precipitation is 800 mm and the mean annual temperature is 27.6°C at Salak station (Suchel, 1988). The year is divided into two main seasons: the wet season from June to September and the dry season from October to May, which is associated with a north to south-west wind, loaded with Saharan dust, called the Harmattan (Kalu, 1979; Suchel, 1988).

The Mandara Mountains are mainly composed of granite and gneiss (Gazel et al., 1956). The sediments found in the Diamaré piedmont were principally deposited during the Quaternary (Hervieu, 1967). They consist mostly of quartz and feldspars, with a decreasing grain-size distribution toward the Yaérés floodplain (Hervieu, 1967). The saprolite, originating from bedrock weathering and occasionally covered by a ferruginous duricrust, is overlain by a clay-rich sediment interfingering with sand lenses (Morin, 2000). Pedogenic

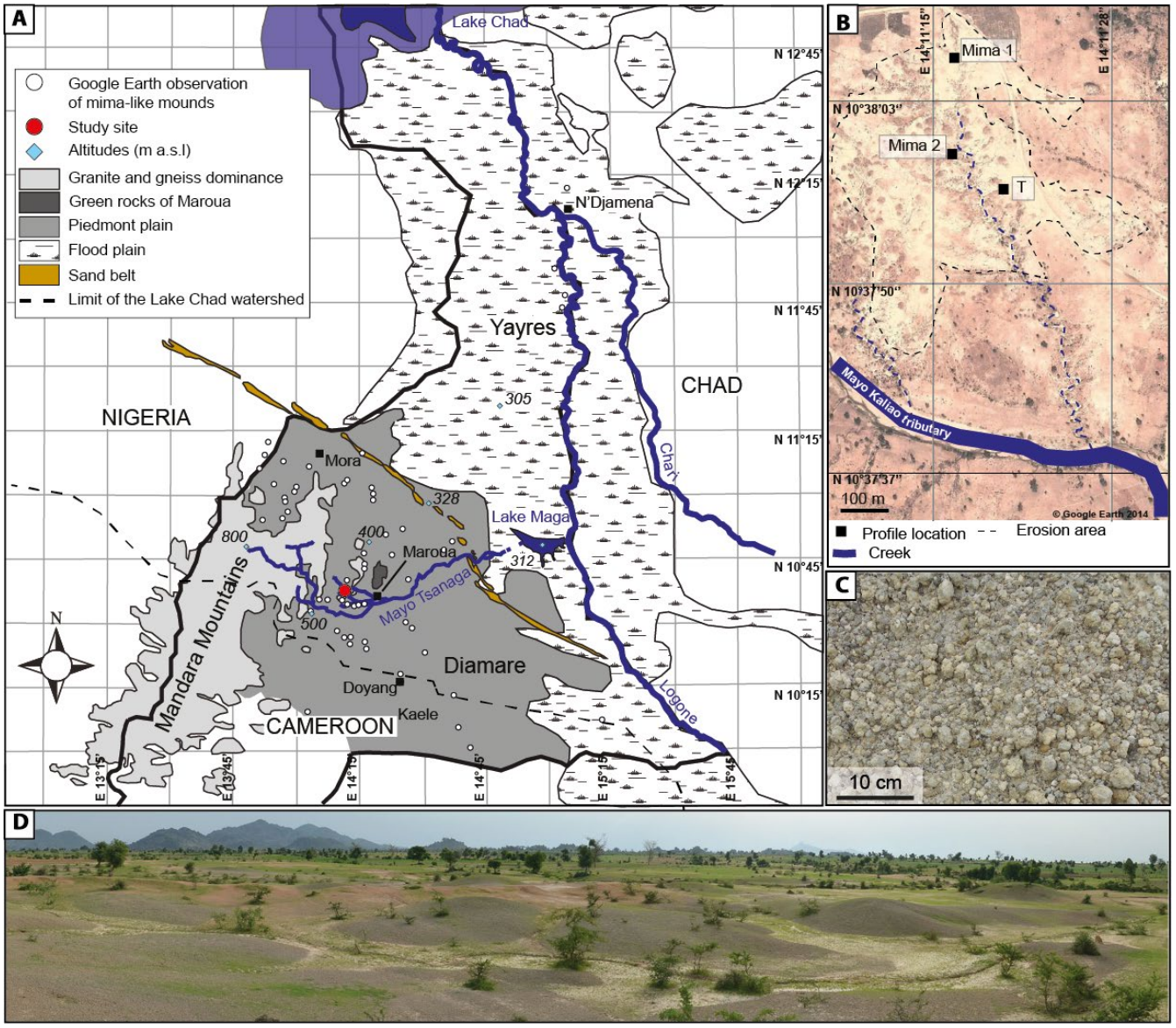

FIGURE 1 Study site location and geological settings. (A) Map of the Far North region of Cameroon, showing the Diamaré piedmont situated between the Mandara Mountains and the Yayres floodplain, separated by a sand belt. Red circle refers to the study and sampling site, located in the Mayo Tsanaga watershed, Chad Lake basin (black dashed line). White circles are Google Earth™ observations of mima-like mounds; black squares are important villages and towns. (B) Google Earth™ view of the study site, highlighting an erosion area (black dashed line) with studied mima-like mounds shown by black squares. (C) Field photograph of an accumulation of carbonate nodules at the soil surface. (D) Photograph of a typical landscape of mima-like mounds, with Mandara Mountains in the background

carbonate nodules are associated with palaeo-Vertisols developed in the clay-rich sediment, called the 'Clay-Rich Parent Material' and have occurred in large areas (CRPM; Diaz et al., 2016a; Dietrich et al., 2017). Nodules accumulate in significant amounts, up to 11 kg/m^2 at the surface and/or within the CRPM (Figure 1C,D; Diaz et al., 2016a).

In the present-day, the palaeo-Vertisols outcrop as peculiar landscape features, such as non-anthropological earth mounds in highly eroded areas, or as whalebacks (Figure 1D). The earth mounds have been described as 'mima-like mounds'. Mima-like mounds are landforms defined in the literature as earth mounds formed by erosion and/or aeolian deposition combined with vegetation patterns (Cramer & Barger, 2014). At this site, they were interpreted as the result of the dislocation of palaeo-Vertisols (Diaz et al., 2016a). The carbonate nodules, collected in the same soil profiles as those studied in this present work, have been dated using radiocarbon, and range from 6.6 to 5.0 ka cal BP (see details in Diaz et al., 2018). The organic matter sequestered in the carbonate nodules has also been dated using radiocarbon and spans from 11.5 to 8.0 ka cal BP. Diaz et al. (2018) concluded that these dates correspond to the time period when organic matter was integrated into the Vertisols. The age of the CRPM deposition has been assessed using OSL dating (applied to K-rich

feldspar grains trapped in nodules; Diaz et al., 2016b) and provided ages ranging from 18.0 to 12.0 ka BP (Diaz et al., 2018). Finally, Dietrich et al. (2017) demonstrated that the CRPM is a 1:1 mixture of the weathered granitic bedrock and Saharan dust using a multi-isotopic approach.

3 | MATERIALS AND METHODS

3.1 | Study site and sample collection

A study site, characterised by important amounts of carbonate nodules and well-developed mima-like mounds, was selected in the granitic area located in the western part of Maroua (Figure 1A through C). An exhaustive field description of the geological settings, including landscape and soils, is given in Diaz et al. (2016a). Only the main characteristics are summarised in this section and presented in Table 1.

Well-developed mima-like mounds formed within the CRPM and outcrops of granitic inselbergs make up the present-day landscape (Figure 1D). The local granite consists of plagioclases, feldspars, quartz and a small amount of biotite (Dietrich et al., 2017). A recent alluvium constituted by reworked CRPM, surrounds the mima-like mounds. The CRPM is observed either (a) in contact with a coarse alluvium (CAL), (b) covered by a fersiallitic pedolith (FP), defined as a reworked soil sediment showing typical features of fersiallitization (Diaz et al., 2016a), or (c) directly in contact with granitic inselbergs.

A trench was dug through two of the mima-like mounds. In the first mima-like mound (Mima 1), the trench was 12 m long and 1.30 m deep. Twelve soil profiles (A–L) were sampled at 5 cm intervals for the first 10 cm from the top, with subsequent samples at depths of every 10 cm (Figure 2). In the second mima-like mound (Mima 2), the CRPM interfingers with the CAL. The trench, dug from the centre to the edge of the mima-like mound, was 5 m long and 1.30 m deep. Five soil profiles (N–P profiles correspond to the CRPM, whereas R and Q profiles are CAL) were sampled using the same strategy as in Mima 1 (Figure 2). Profile T was sampled in the FP close to Mima 1 and 2 (Figure 1B). Two different layers were observed: (a) the FP (samples T1–T4) overlaying (b) the CRPM (samples T6–T10). The sampling strategy was the same as for Mima 1 and 2. Nodules were sampled at the soil surface and in soil horizons. Finally, a sample of granite was collected from a neighbouring inselberg. A detailed sketch of the sample locations in the two mima-like mounds is given in Figure 2.

3.2 | Analytical methods

Soil samples were sieved at 2 mm and all of the samples (soil fine earth, carbonate nodules and granite) were crushed in an agate mortar. The chemical compositions of these bulk samples were determined using X-ray fluorescence (XRF) on glass pellets after $LiBO_2$ fusion using a XRF PANalytical Axios spectrometer. The detection limit is reported as <5 ppm. The carbonate contents of soil fine earth and carbonate nodules were measured using the mass loss method with 2.2 M acetic acid on 2 g of sample. Triplicates performed on five samples validated the method showing a maximum relative standard deviation (RSD) of 5.7%. An extraction using 0.0166 M cobaltihexamine was performed on soil fine earth to determine the CEC and the exchangeable cations (Na^+, K^+, Ca^{2+}, Mg^{2+} and Al^{3+}), following the protocol established by Ciesielski et al. (1997). The concentrations of the various exchangeable cations and cobalt were measured using inductively coupled plasma-atomic emission spectroscopy (ICP-OES; Perkin Elmer ICP-OES Optima 8300). The detection limit was <100 ppb for Na, K, Ca, Mg, Al and Co, respectively, with a repeatability <10% based on triplicate tests (in extractions as well as measurements) with three random samples. The cobaltihexamine was preferred to ammonium

TABLE 1 Description of profiles and samples from Diaz et al. (2016a)

Material	Samples	Texture	Structure	Skeleton	pH_2O	Mineralogy
Clay-rich parental material—CRPM	Profiles B to L (Mima 1). Profiles N and O (Mima 2) and samples T6 to T10	Clay-loam	Massive	Up to 15% carbonate nodules, a few nodules of Fe-Mn oxides	8.1–9.6	qtz > phyl (sm, kao, ilt) > K-f > plg
Coarse alluvium—CAL	Profiles Q and R (Mima 2)	Sandy loam	Single grain	Up to 30% silicate gravels	7.5–8.2	qtz > K-f > phyl >plg
Recent alluvium—A	Profile A (Mima 1)	Silt loam	Massive	—	8.4–9.0	qtz > K-f > phyl >plg
Fersiallitic pedolith–FP	T1–T4	Sandy loam	Angular blocky	—	7.2–7.6	qtz > phyl (kao > sm) > K-f > plg

pH_2O was measured in the laboratory with a pH meter.

Abbreviations: qtz: quartz; phyl: phyllosilicate; K-f: K-feldspar; plg: plagioclase; sm: smectite; kao: kaolinite; ilt: ilite. Total organic carbon < 0.5% in all profiles.

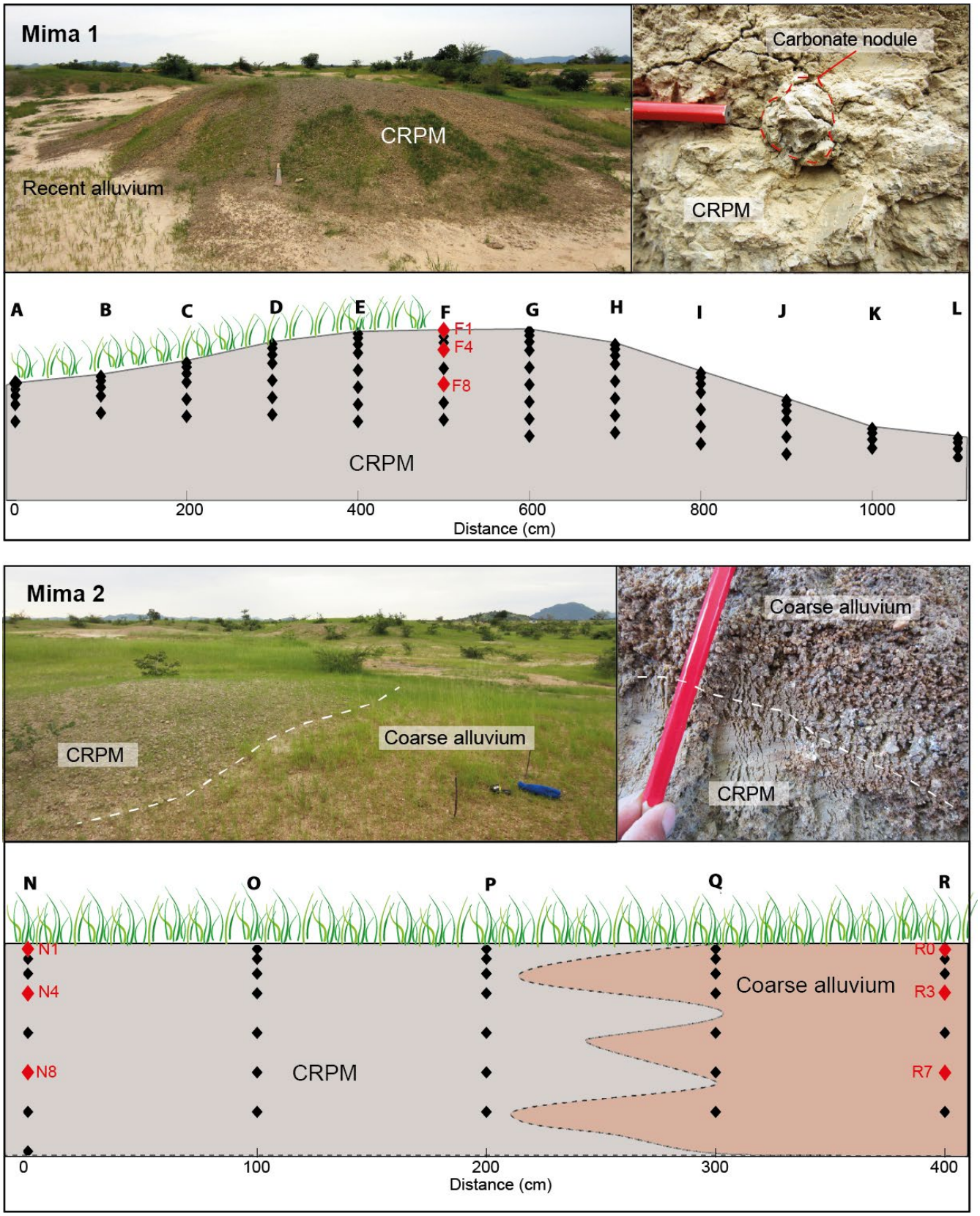

FIGURE 2 Distribution of samples in the mima-like mounds. Mima-like mound 1 is composed of the clay-rich parent material (CRPM) surrounded by a recent alluvium and covered by carbonate nodules. The top-right picture shows a detail of the soil profile: the CRPM includes a carbonate nodule in the soil (1 m deep). In the mima-like mound 2, the CRPM interfingers the coarse alluvium. Black and red diamonds indicate the sample locations, the red ones referring to those selected for the extraction procedure

TABLE 2 Results of the principal component analysis

	End member 1		End member 2			End member 3
	Na_2O	K_2O	Al_2O_3	Fe_2O_3	MgO	CaO
PC1	−0.269	−0.069	−0.442	−0.251	−0.092	0.836
PC2	−0.771	−0.951	0.851	0.944	0.955	0.316

The correlation coefficients between the two first principal components (PC1 and PC2) and each variable are given in this table. The correlation coefficient values are used to project the variables in a circle of radius = 1: the closest variables are clustered into three groups in order to define three geochemical attractors or end members: end member 1 (Na_2O and K_2O), end member 2 (Al_2O_3, Fe_2O_3 and MgO), and end member 3 (CaO).

acetate or barium chloride, as it does not dissolve the carbonate (Dohrmann & Kaufhold, 2009). The density of carbonate nodules was assessed on five samples using the cylinder method, which consists of putting a sample, whose mass is known (m), in a known volume of water and looking at the volume displacement (V) with the cylinder graduation: the bulk density is given by the ratio m/V.

Ten soil samples with six associated nodules (when present in these 10 samples) and five surface nodules were selected for trace element and REE analyses (samples in red in Figure 2). Measurements were performed on two different fractions (leading to 42 measurements): (a) a dissolved carbonate phase obtained by a 2.2 M acetic acid extraction (Arunchalam et al., 1996), and (b) the residual phase, which was not dissolved during the acid acetic extraction. A solution of 2:1 HNO_3:HF was used to put this residual phase completely into solution. The granite and the FP (samples T1–T4) were analysed after total dissolution in 1:1 HNO_3:HF. All chemical treatments were performed in a clean-laboratory (class 1000) using bi-distilled acids. Major, trace element and REE concentrations from the dissolved sample fractions were measured with an inductively coupled plasma-mass spectrometer (ICP-MS; Element XR) at the Institute of Earth Sciences (University of Lausanne), with an intermediate precision <5%. All soil samples were only partially dissolved after the 2:1 HNO_3:HF attack, whereas the residual phases of the carbonate nodule samples were totally dissolved. Therefore, the residual phases of the soil samples were analysed using a complementary method: these phases were fused in $LiBO_2$ and the resulting glass pellets were analysed using a Laser Ablation ICP-MS (Agilent 7700 coupled with GeoLas 200MArF excimer) in order to measure their mass fraction in major and trace elements. Triplicate analyses were performed on a nodule sample in order to control the repeatability of the acid acetic extractions. Results give a maximum RSD of 5% for major and trace elements (see Supplementary Material A). The Ce anomaly (Ce/Ce*) was calculated using the following equation (Equation 2, Braun et al., 1998):

$$\frac{Ce}{Ce^*} = \frac{\frac{[Ce_{sample}]}{[Ce_{granite}]}}{\sqrt[2]{\frac{[La_{sample}]}{[La_{granite}]}} \times \sqrt[2]{\frac{[Pr_{sample}]}{[Pr_{granite}]}}} \quad (2)$$

The local granite was chosen for the normalisation, instead of the chondrite or the Upper Continental Crust, as it is the dominant bedrock in the watershed (Gazel et al., 1956). The La/Yb ratio was calculated to estimate the fractionation between LREE and HREE.

3.3 | Data processing

Principal component analyses (PCA) and cluster analyses (CA) were performed on the soils' major elements expressed as oxides (Na_2O, K_2O, MgO, CaO, TiO_2, MnO, Fe_2O_3, Al_2O_3 and SiO_2; see Supplementary Material B), using Matlab® software. Data were standardised and CA were performed using the Euclidian distance and the Ward agglomeration algorithm. Pearson correlation coefficients (r, Table 2) of the two first principal components (that explain >80% of the total variance) with the variables were calculated as follows: $r = \lambda_i \sqrt{u_i}$, where u_i the matrix of the respective eigenvectors and λ_i the matrix of their associated eigenvalues. These r coefficients were used to define the three main geochemical attractors or end members (EM), which are EM 1 = K_2O+Na_2O, EM 2 = Al_2O_3+Fe_2O_3+MgO and EM 3=CaO. The SiO_2 variable was excluded, as it is a common element of silicates and therefore not discriminant. In order to plot the samples in a ternary plot defined by the three end members, the sum of EM 1 = K_2O+Na_2O, EM 2 = Al_2O_3+Fe_2O_3 + MgO and EM 3 = CaO was normalised to 1 (100%). In addition, in this ternary plot, the samples were grouped by different symbols using CA (Figure 3). Finally, carbonate nodules and granite samples were added to the ternary plot.

4 | RESULTS

The cluster analysis, based on major element compositions, allocated soil samples to five different groups (Figure 3). The first group refers to the coarse alluvium (CAL, n = 13, samples from R and Q profiles), whereas the FP (T1–T6) constitutes the second group with a sample of recent alluvium (A1; n = 6). A1 is located at the edge of Mima 1 and is clearly reworked material. Samples from the CRPM are divided into three different groups: samples close to the surface at the

centre of Mima 1, named C-CRPM (n = 12), the remaining samples of Mima 1, named M1-CRPM (n = 64), and samples from the CRPM of Mima 2, named M2-CRPM (n = 23). All soil samples have a bulk composition dominated by the Al_2O_3+Fe_2O_3+MgO end member (in a proportion of between 70% and 90%), but some outliers remain (Figure 3). The CAL, FP and A1 samples display the highest K_2O and Na_2O contents and are therefore the closest to the composition of the granite. The M1-CRPM samples have the highest amount of Al_2O_3+Fe_2O_3+MgO, whereas C-CRPM samples have the highest amount of CaO.

In addition to the major element compositions, two main compartments of exchangeable Ca have also been considered: the diffuse soil carbonate (excluding nodules), which is also a sink for Ca, and the CEC fraction. The carbonate content of the CRPM ranges from 0.5% to 5.8% with maximum values at the centre of Mima 1. However, CAL and FP have lower values ranging from 0% to 2.4% (Figure 4). The CEC and the exchangeable Ca display concomitant variations in the various sedimentary components of the landscape (Figure 4). In the CRPM, CEC and the exchangeable Ca values range from 16 to 43 $cmol^+$/kg, and from 7 to 21 $cmol^+$/kg (Ca represents between 36% and 70% of the total CEC), respectively. In the CAL and FP, values range from 8 to 20 $cmol^+$/kg for the CEC, and from 2 to 12 $cmol^+$/kg for the exchangeable Ca (Ca represents between 16% and 50% of the total CEC).

On average, the nodules consist of 70% low-Mg calcite and 30% of a residual silicate phase. Observations of carbonate nodules in thin section emphasise their micritic nature (Figure 5). Two different distribution patterns are observed (Stoops, 2003): a random pattern defined as open-porphyric, coarse-fine related distribution (grains are mainly quartz, plagioclases and K-feldspar) and a fan-like pattern including less silicate grains. Septarian cracks are partially infilled or coated with sparitic calcitic cements. The geochemical composition of the carbonate fraction in nodules is homogeneous with a low variance (average RSD is 25%), despite the fact that data include nodules from both surface and deep soil (n = 11; Figure 6). Carbonate nodules show clear enrichments in Ca, Mg, Sr, Y, U and REE, whereas they are strongly depleted in Al, Na, K, Fe, Ti, Zr, Rb and Ce (Figure 4). The sum of REE is the highest among all the other samples, their La/Yb ratios are >1, and they have Ce/Ce* values <1 (Figures 4 and 6).

Aside from the bulk sample analyses given above, analyses of the residue fractions from the CRPM, the CAL and the FP, display similar trends, but with some differences in terms of amplitude (Figure 6). These trends refer to a composition close to Saharan dust. The CRPM, the CAL and the FP are mainly depleted in Ca and Na, and enriched in Fe, Mg, Mn, Ti, Zr, V and Y. The enrichment in Fe, Mg, V and Mn is more important in the CRPM compared to the CAL and the FP, whereas FP has the highest enrichment in Zr and Ti. As discussed above, the composition of CAL is closest to

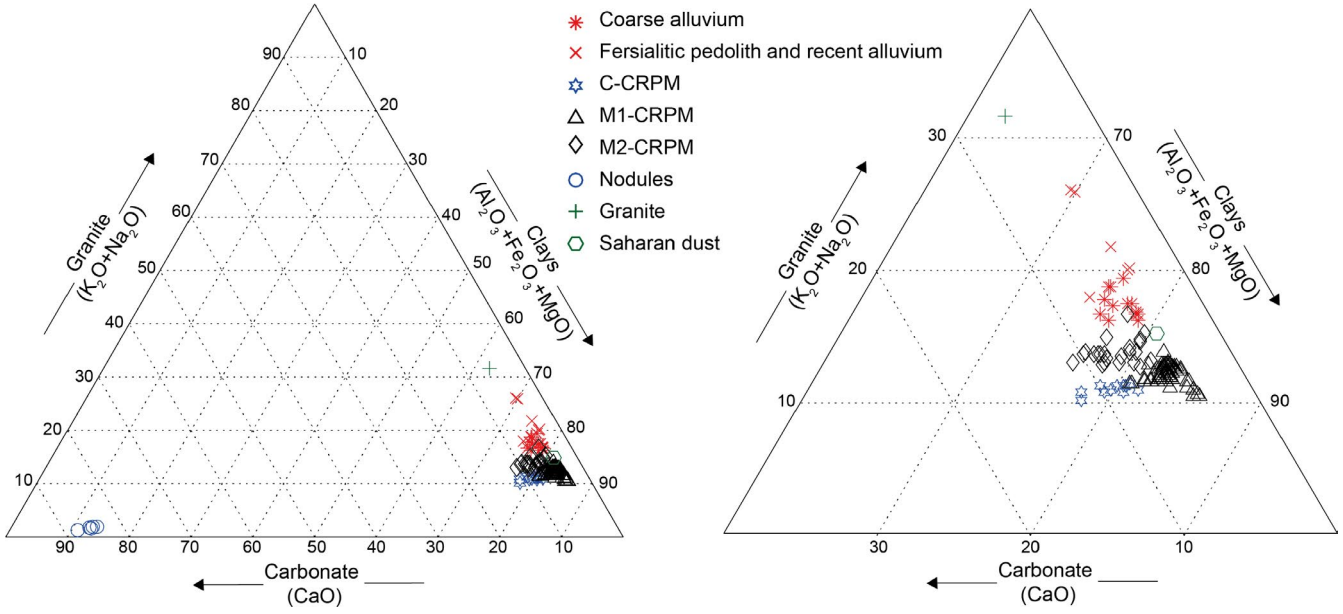

FIGURE 3 Geochemical ternary plot of XRF data obtained in bulk soil samples, carbonate nodules, dust and granite. The ternary plot on the left-hand side displays the samples within the full variation span; the right-hand side plot is a close-up of the sample distribution without the nodules (which have a CaO content >80%). The three end members have been chosen according to their correlations with the first two principal components after PCA. Sample colour codes refer to five different sample groups according to a cluster analysis: group 1 denotes the coarse alluvium (n = 13, samples from R and Q profiles), group 2 corresponds to the fersiallitic pedolith and recent alluvium (n = 6, samples T1–T6, and A1), group 3 to samples from the centre of Mima 1 (n = 12), group 4 to the other samples of Mima 1 (n = 64), and finally group 5 to samples from Mima 2 (n = 23). Granite, Saharan dust and nodules are also displayed in the ternary plot, but they were not used in the cluster analysis

the granite. All these sediments are characterised by a slight enrichment in REE, especially in HREE. The sum of REE normalised to the granite is close to 1, the La/Yb ratio <1, with the lowest values in the FP, and with a positive Ce/Ce* anomaly (Figure 4).

5 | DISCUSSION

5.1 | Identifying the past compartments in the present-day landscape

5.1.1 | The calcium sources: Granitic bedrock and dust

The K_2O+Na_2O end member of the ternary plot (Figure 3) reflects the silicate minerals which make up the granite (i.e. K-feldspars and plagioclases). The CAL and FP samples, which are characterised by grain-size modes of coarse-medium sand and coarse silt, are the closest to this end member. These grain sizes are typical of arenaceous saprolites (Eswaran & Bin, 1978; Evans & Bothner, 1993; Migoń & Thomas, 2002).

The main difference in the geochemical composition of CAL and FP lies in the slight depletion in Ca and Na (Figure 6) compared to granite. This is due to plagioclase hydrolysis, one of the first minerals to be weathered in this rock type (Fedo et al., 1995; Nesbitt & Markovics, 1997; Nesbitt & Young, 1984). This depletion in Ca and Na leads to a relative enrichment in other elements, such as Fe, Mg, Mn, V, Y and especially Ti and Zr. The latter two elements are the main components of two of the most resistant minerals found in granite (i.e. rutile and zircon; Schaetzl & Thompson, 2015). This concentration of resistant minerals also leads to an enrichment in HREE, with respect to LREE, and a La/Yb ratio <1 (Figures 4 and 6), as HREE are mainly associated with them (Braun et al., 1998; Laveuf & Cornu, 2009; Nickel, 1973). Therefore, the primary minerals inherited from the granitic arena characterise both CAL and FP. However, FP not only experienced hydrolysis, but also fersiallitization,

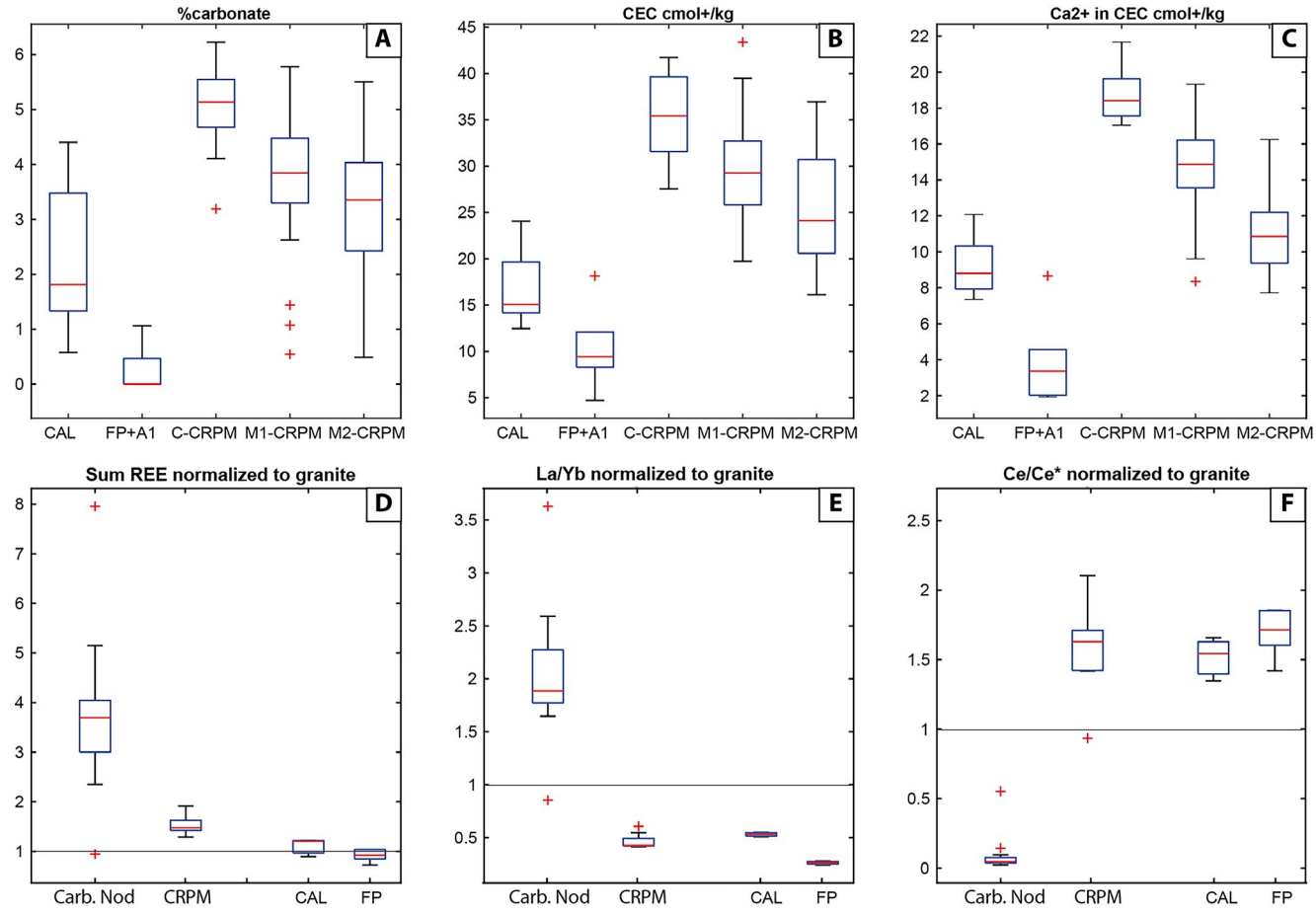

FIGURE 4 FIGBoxplots of Ca-related and REE-related parameters. Mid-line is the median, edges of the box are 25 and 75 percentiles, respectively, and the whiskers refer to the 10 and 90 percentiles. Red crosses are outliers. A–C: boxplots of each group obtained using cluster analysis: (A) carbonate; (B) cation exchange capacity; (C) exchangeable Ca. D–F: (D) sum of REE; (E) La/Yb; (F) Ce/Ce*. Data are adjusted to the respective carbonate content of the sample and normalised using local granite composition. Samples have been grouped as follows: carbonate nodules (Carb. Nod, $n = 11$), soil residue (CRPM; $n = 9$), coarse alluvium (CAL; $n = 3$) and fersiallitic pedolith (FP; $n = 4$)

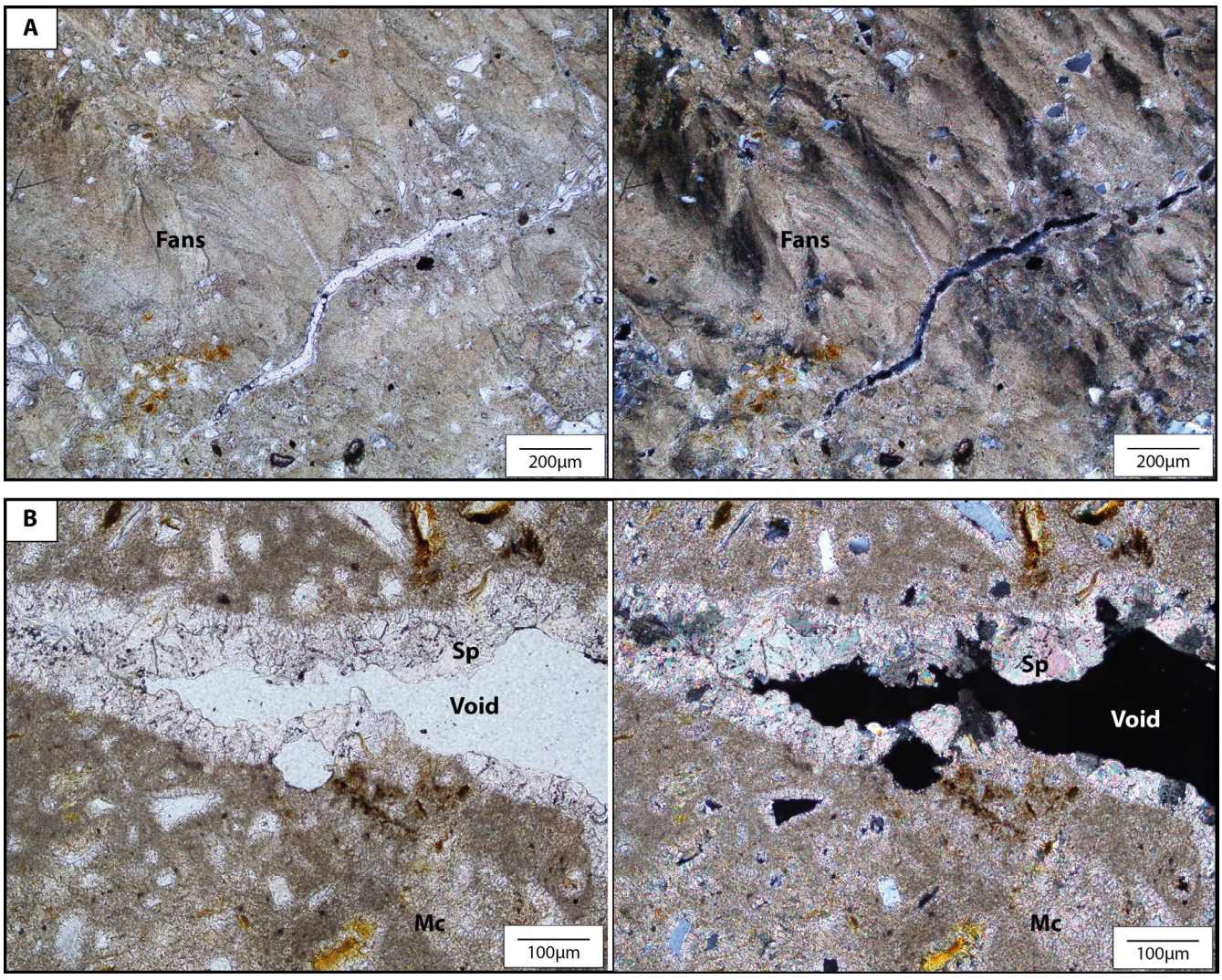

FIGURE 5 Photomicrographs of a carbonate nodule observed in thin section. Abbreviations: sp—sparitic calcite; mc—micritic calcite. Left: plane polarised light; right: crossed polarised light. (A) Carbonate nodule showing a fan-like cement. This type of calcitic fabric contains only rare silicate grains. (B) Carbonate nodule showing (a) silicate grains entrapped in micrite, (b) a sparitic cement is coating a void and (c) aureoled quartz with microsparite

before it was reworked. Indeed, FP contains not only primary silicate minerals, but also clays (essentially kaolinite with a minor proportion of smectite) and Fe oxyhydroxides, which point to the typical features of fersiallitization observed in thin sections (Diaz et al., 2016a; Marcelino et al., 2018).

Dietrich et al. (2017) found that Saharan dust is the other main source of Ca. Because Recent dust deposits were not sampled during this study, the geochemical composition of Saharan dust has to be estimated from the literature. No data are available for recent dust composition collected in the North Cameroon area. The best fitted data would be the geochemical composition of dust at the time of CRPM deposition (18.0 to 12.0 ka BP, Diaz et al., 2018), data which are not available. Nevertheless, when considering the present-day back trajectories of air masses, it appears that the Bodélé depression is the main source of dust for the Far North of Cameroon (Skonieczny et al., 2001). Therefore, it can be hypothesised that at the time the CRPM was deposited the sources could have been comparable, justifying selection of the soils/sediments of the Bodélé depression for comparative purposes. Importantly, many dust samples are soils or sediments, and not dust sampled from dust sampling collectors. Bristow et al. (2020) proposed a data set with quite a homogenous geochemical composition, but it does not include REE. Data from Abouchami et al. (2013) show an important heterogeneity in the Ca content in samples from the Bodélé depression. The Ca content in dust is closely related to the calcite content and this mineral is not transported over large areas and long distances (Scheuvens et al., 2013). In order to reduce the heterogeneity in the data of Abouchami et al. (2013), two outlier samples with very high Ca contents (higher by a factor of 10 compared to other samples) were excluded from the data set. Therefore, an average composition of Saharan dust (10 samples) was calculated using

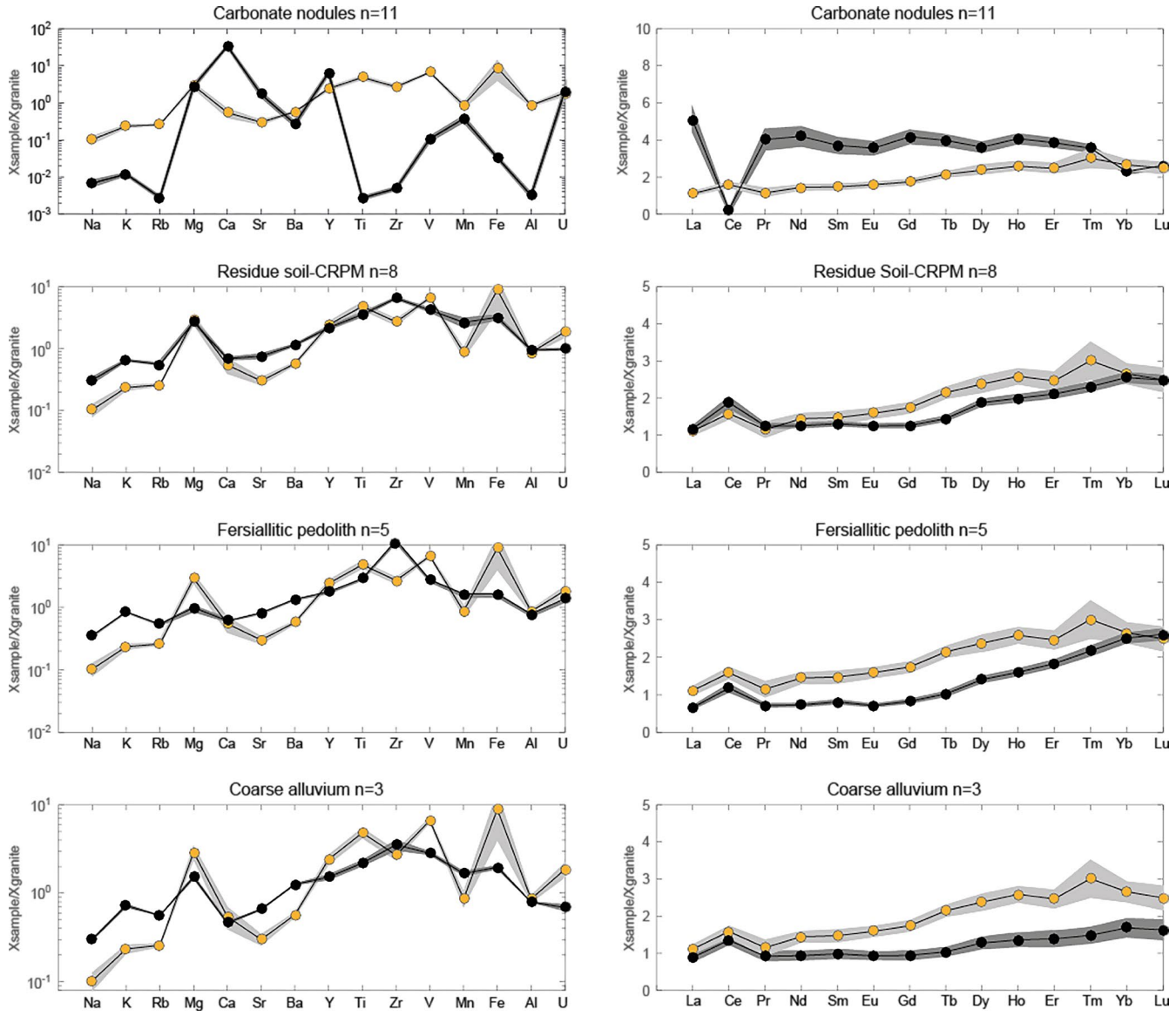

FIGURE 6 FIGComparison of the geochemical compositions of carbonate and residual fractions (black dots) with respect to Saharan dust (orange dots). Results are normalised to the local granite composition. Samples have been grouped as follows: carbonate nodules ($n = 11$), soil residue-CRPM ($n = 8$), coarse alluvium ($n = 3$) and fersiallitic pedolith ($n = 5$). Samples from each group have been averaged. The average is displayed with a black line and the standard error is given within the dark grey shaded area. The Saharan dust profile is shown on each plot to facilitate a comparison with the carbonate and residual fractions. The Saharan dust profile represents the average values calculated using data from the literature (see text) and the light shaded area denotes the standard error

geochemical data of the Bodélé depression reported from four different studies (i.e. Moreno et al. 2006 $n = 2$, Castillo et al. 2008 $n = 1$, Abouchami et al. 2013 $n = 5$ and Gross et al. 2016 $n = 2$). The results are plotted with their respective standard error (Figure 6). The Saharan dust composition has been standardised to granite.

FIGURE 7 (A) Ca location in a soil profile through time. Ca is transferred from granite and dust sources to carbonate nodules, highlighting the role of Vertisols as traps of Ca and C. This sketch includes a saprolite formation before the CRPM implementation, that is, before 20 ka cal BP. In Far North Cameroon, wet climate conditions, which led to Ferralsol formation (pedogenesis I), have been reported from 29 ± 1 to 26 ± 1 ka cal BP (Hervieu, 1967; Maley, 1981). Pedogenesis I is ferrallitization and pedogenesis II is vertisolization. CRPM for Clay-Rich Parent Material, AHP for the African Humid Period, dated between 14.8 and 5.5 ka cal BP (deMenocal et al., 2000). *Dating from Diaz et al. (2018). (B) Ca location in the various compartments of the landscape. Upstream, pedogenesis is dominated by monosiallitisation (in this case, resulting in the development of fersiallitic soils), whereas, downstream, bisiallitisation and accumulation of sediments and cations occur, resulting in the genesis of Vertisols (following the model proposed by Bocquier, 1971). Q is used for Ca sources, C for Ca transient compartments, TC for the Ca-trapping compartment, and the arrows represent fluxes. Sources, sinks, transient compartments and fluxes/exchanges are used in the sense given by Schlesinger and Bernhardt (2013)

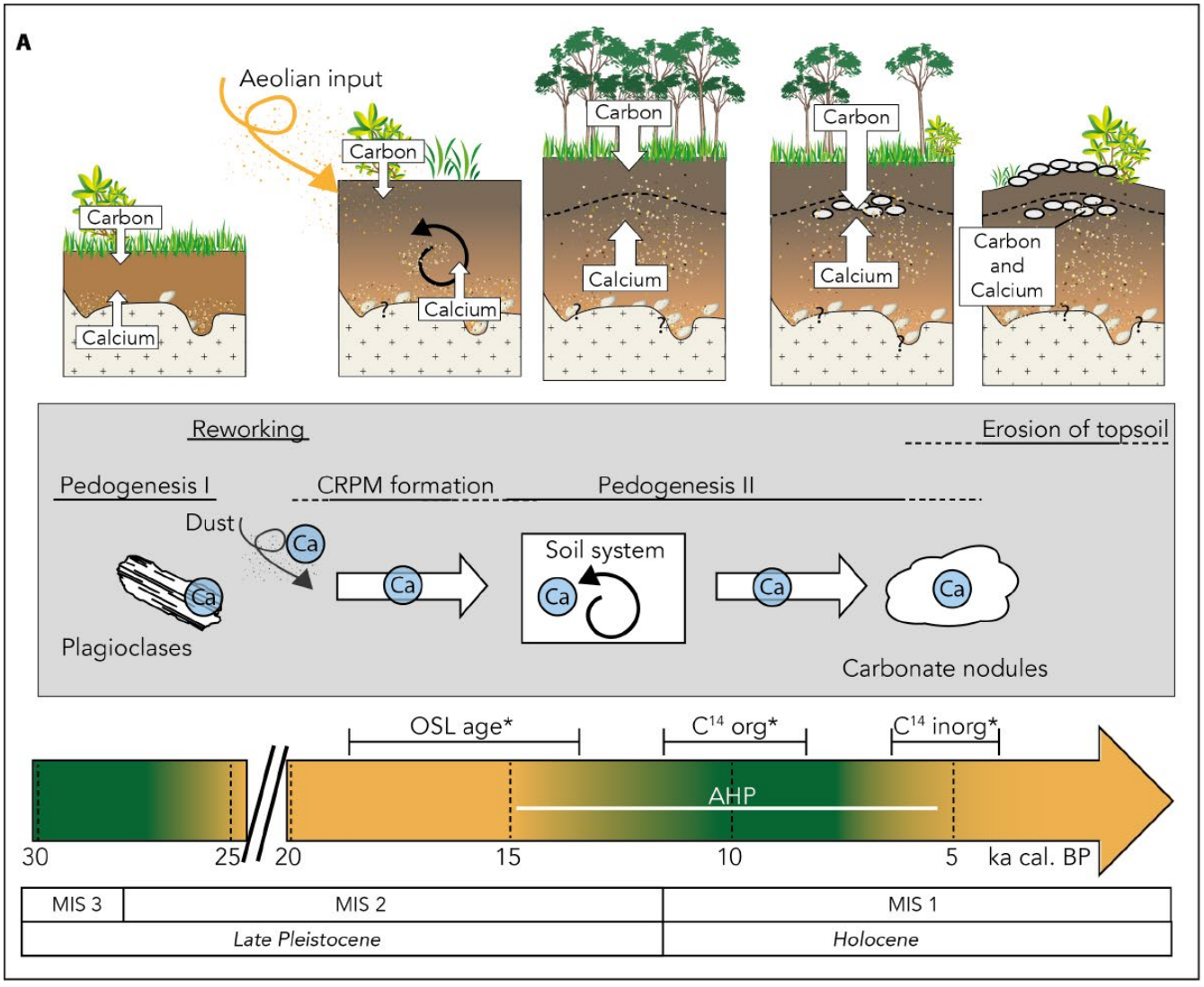

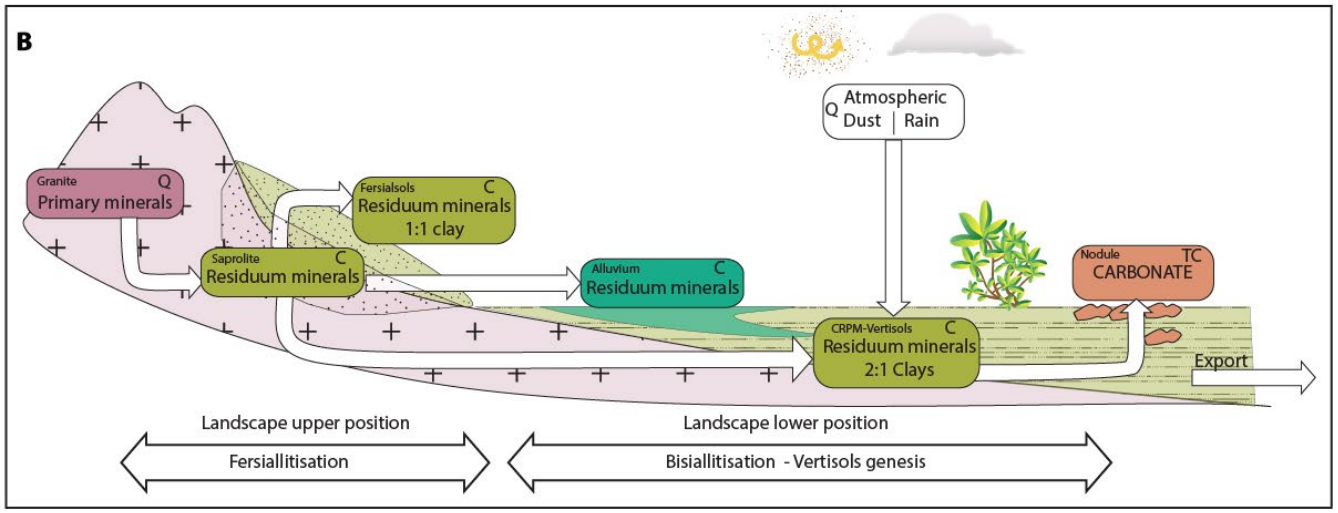

The Mg, Fe, Ti, Zr, V and some REE mass fractions are higher for the Saharan dust than the granite, but those of Ca, Sr, Na, K and Rb are lower. Calcium in dust can originate from a number of mineral phases. Indeed, Saharan dust mineralogy can include plagioclases, hornblende, calcite and apatite (Scheuvens et al., 2013), which are Ca-bearing minerals. In addition, Ca can also be sorbed on 2:1 clays or adsorbed on 1:1 clays in minor amounts. These minerals were

mixed with saprolite during deposition of the CRPM between 18.0 and 12.0 ka cal BP (Diaz et al., 2018; Dietrich et al., 2017). Later, Ca was released during weathering (Figure 7A).

5.1.2 | Transient compartments: Vertisols developed in the CRPM

The Al_2O_3+F_2O_3+MgO (EM2) end member of the ternary plot (Figure 3) is related to the weathering products, as these three elements are often identified in clay minerals and/or oxides. Samples C-CRPM, M1-CRPM and M2-CRPM are dominated by a clay-loam texture and these sample groups are the closest to the EM2 end member. Indeed, smectites and kaolinite have been identified in the CRPM (Diaz et al., 2016a). The high aluminium (Al) content in the CRPM results from its limited mobility, as this element is transferred from primary minerals to secondary clay minerals. Aluminium can contribute to kaolinite formation as well as Mg-smectites (Clauer & Paquet, 1997). The presence of 2:1 clays promotes enrichment in Fe and Mg. In Vertisols from Sudan, 75%–100% of the Fe(III) is related to Fe-beideillite, a phyllosilicate of the smectite group (Blokhuis, 1993). Magnesium can also be a component of smectite (Kabata-Pendias & Pendias, 2011). In addition, oxyhydroxides concentrate Fe, as well as Mn and V, as these elements are easily incorporated into this group of minerals (Bigham et al., 2002; Schwertmann & Taylor, 1989). The CRPM also displays an enrichment in REE, especially in HREE, compared to granite and this enrichment is higher when compared to the FP and CAL (Figures 4 and 6). This enrichment is probably related to the abundance of clays and oxides, as REE sorption is a common process in such minerals (Compton et al., 2003; Coppin et al., 2002). Moreover, the CRPM has a higher pH than FP and CAL. Indeed, the pH is a crucial parameter for HREE accumulation, as HREE solubility increases with decreasing pH (Aubert et al., 2001; Cao et al., 2001; Compton et al., 2003; Sako et al., 2009). Additionally, this enrichment in HREE compared to the granite can also be due to the presence of some Saharan dust in the CRPM, which is itself enriched in HREE.

The presence of 2:1 clays and oxides in the CRPM has an important influence on Ca. The CRPM has a higher CEC and Ca exchangeable content than FP and CAL (Figure 4) due to the presence of 2:1 clays (Blokhuis, 1993; Clauer & Paquet, 1997). To a lesser extent, oxides and oxyhydroxides (Fe and Mn oxides in this case) also contribute to high CEC (Schaetzl & Thompson, 2015). Finally, other transient compartments exist for Ca, that is, the vegetation and the soil organic matter (Rowley et al., 2018; with a turnover of about a few years; Dincher et al., 2020; Turpault et al., 2019). The vegetation must have been mostly woody during the African Humid Period in North Cameroon (Amaral et al., 2013; Diaz et al., 2018) and represented an effective Ca transient compartment. During this humid period, Vertisols provided some reducing conditions due to their high soil water content, preserving some of this organic matter (Mermut et al., 1996; Southard et al., 2011). This preserved organic matter probably contributed to transient Ca pools. Therefore, Vertisols developed in the CRPM seem to be a suitable location to accumulate Ca and to act as a transient compartment for Ca (Figure 7A).

5.1.3 | The Ca sink: Carbonate nodules and soil carbonate

Carbonate nodules are common features of Vertisols (Kovda et al., 2006; Wieder & Yaalon, 1982), but mechanisms leading to their formation are still under debate (Zamanian et al., 2016). Conditions in Vertisols in the Far North of Cameroon obviously provided ideal settings for nodule formation as shown by their great abundance. Calcium and (bi)carbonate ions were present in the soil as reported above. Calcium originated from plagioclase weathering and dust deposits (Dietrich et al., 2017), while C stemmed from soil respiration (Cerling, 1984; Hasinger et al., 2015). In addition, the pH of the CRPM was probably alkaline enough to promote calcite precipitation, a condition that is documented below using REE.

High pH favours REE accumulation (Aubert et al., 2001; Cao et al., 2001; Compton et al., 2003; Sako et al., 2009). Rare earth element complexation with carbonate is maximised when the pH value is 10 (Pourret et al., 2007), providing an explanation for the higher REE content observed in the carbonate phases than in the silicate sediments (Figure 4). Moreover, because of the closeness of Ca^{2+} and REE^{3+} ionic radii, REE can be incorporated into carbonate minerals, notably through isomorphic exchange of Ca^{2+} in the calcite lattice, although the compensation of the charge imbalance (2+ vs. 3+) is not yet clearly understood (Laveuf & Cornu, 2009). Carbonate nodules are also characterised by a strong negative Ce anomaly (Figure 4), as previously reported in the literature (Huang & Wang, 2004; Violette et al., 2010a). This attribute indicates that, when carbonate precipitated, the conditions were oxic and only scarce Ce was available, as Ce remains trapped in its cerianite form (Braun et al., 1990, 1998; Mongelli, 1997), as shown by the positive Ce anomaly recorded in the CRPM.

Moreover, Vertisols underwent important variations in soil water content during the year (Coulombe et al., 1996; Kutílek et al., 1996). All of the radiocarbon ages of the carbonate nodules range between 6.6 and 5 ky BP cal (Diaz et al., 2018). This period corresponds to the end of the African Humid Period, when climate conditions became drier (Amaral et al., 2013; de Menocal et al., 2000; Garcin et al., 2018; Shanahan et al., 2015), resulting in decreased

soil moisture. Consequently, calcium carbonate dynamics were impacted in two different ways: (a) the precipitation of carbonate nodules was promoted, and (b) the dissolution of carbonate nodules was reduced, enhancing their preservation inside the soil.

Based on the various profiles and samples, it is now possible to reconstruct the past landscape using the top of sequence concept proposed by Bocquier (1971). In upper topographic positions, the soil mineralogy is mainly composed of silicate primary minerals, kaolinite and Fe oxyhydroxides, pointing to fersiallitization processes and resulting in a depletion of alkaline elements. In contrast, downstream, bisiallitisation is the main operative process, leading to the formation of 2:1 clays, resulting in an enrichment of alkaline elements. Consequently, the FP can be considered as a product of shallower weathering formed at the same time as Vertisols. Therefore, an important part of the Ca present in the watershed has been transferred from granite and dust sources to carbonate nodules. With time, the Vertisol geosystem has been partly fossilised and Ca, which was transferred from the transient compartment (2:1 clays and oxides of the CRPM, vegetation and organic matter) to carbonate nodules, remained sequestered until today (Figure 7B), as evidenced by significant amounts of carbonate nodules observed in the present-day surface landscape (11 kg of nodules per m^2; Diaz et al., 2016a).

5.2 | Calcium accumulation in mima-like mounds and its impact on the Ca balance: A quantitative assessment

5.2.1 | Calculations of respective Ca depletion and accumulation

Calcium depletion and accumulation have been calculated by comparing the palaeo-Vertisols and their parental material with respect to density and volume variations. For this purpose, palaeo-Vertisols have been divided into three groups: carbonate nodules, soil micritic carbonate (sink) and soil residue (transient), hereafter noted Nod, SCarb, and Res, respectively, the parent material (sources) being noted as PM.

The parent material of palaeo-Vertisols is the CRPM, which is approximately a 1:1 mixture of Saharan dust and granitic saprolite (Dietrich et al., 2017). A rough assessment of the initial geochemical composition of the CRPM (i.e. before Vertisol development, as an unweathered material) can be calculated by averaging the composition of Saharan dust (median from literature) and saprolite. Coarse alluvium was defined above as the residuum of a weathered granite and has been used as an equivalent of the composition of the saprolite. Regarding the saprolite, Begonha and Braga (2002) propose a density of 1.5 g/cm^3, and the density of dust was chosen as 1.65 g/cm^3, a conventional density for desert loess (Pye, 1987). However, calculations were also performed considering the granite as the parent material in order to compare the CRPM with a simpler end member.

First, the Ca depletion between the parent material and the palaeo-Vertisols' residue is calculated normalising to an immobile element. Titanium was chosen as it is generally preserved and remains unchanged in Vertisols (Stiles et al., 2003). As ratios are calculated, that is, Ca/Ti, densities and volumetric changes do not need to be considered, and the percentage of Ca depletion/accumulation can be calculated using the following equation (Equation 3):

$$\%\mathrm{Ca}_{\mathrm{Res}} = \frac{[\mathrm{Ca}]_{\mathrm{Res}}/[\mathrm{Ti}]_{\mathrm{Res}}}{[\mathrm{Ca}]_{\mathrm{PM}}/[\mathrm{Ti}]_{\mathrm{PM}}} \quad (3)$$

Calcium accumulation inside the carbonate phase of palaeo-Vertisols (i.e. soil carbonate and carbonate nodules, as Ca sinks) has to be estimated as well. However, it is not possible to normalise to an immobile element, as it is not applicable to carbonate phases, because they are secondary in origin. It is possible to circumvent this problem by comparing one cubic metre of parent material with one cubic metre of palaeo-Vertisols. These calculations must account for the density and volume variations. The nodule density was measured as 2.2 ± 0.1 g/cm^3. Densities of soil fine earth were not measured, but data are available in the literature: Lamotte et al. (1997) measured a density between 1.8 and 1.9 g/cm^3 for solodic Planosol, and Peltier (1993) gave values between 1.5 and 1.9 g/cm^3 for palaeo-Vertisols from the Far North region of Cameroon. Therefore, a density of 1.7 g/cm^3 was chosen for the palaeo-Vertisols residue, while 2.7 g/cm^3 was chosen for the density of soil carbonate as the carbonate soil precipitated as micrite. A calculation of a volumetric strain (ε) is proposed by Egli and Fitze (2000) and this value was used to correct the volume of the present-day palaeo-Vertisols (Equation 4).

$$\varepsilon = \frac{(\rho_{\mathrm{PM}} \times [\mathrm{Ti}]_{\mathrm{PM}})}{(\rho_{\mathrm{Res}} \times [\mathrm{Ti}]_{\mathrm{Res}})} \quad (4)$$

Calcium accumulation in carbonate phases can be then calculated using Equations (5) and (6), for micritic carbonate in the soil ($\%\mathrm{Ca}_{\mathrm{SCarb}}$) and carbonate nodules ($\%\mathrm{Ca}_{\mathrm{Nod}}$), respectively. The sum of the two carbonate phases gives the total Ca accumulation in the palaeo-Vertisols (Equation 7).

$$\%\mathrm{Ca}_{\mathrm{SCarb}} = \frac{\alpha_{\mathrm{SCarb}} \times [\mathrm{Ca}]_{\mathrm{SCarb}} \times \rho_{\mathrm{SCarb}}}{\alpha_{\mathrm{Res}} \times [\mathrm{Ca}]_{\mathrm{PM}} \times \rho_{\mathrm{PM}}} \times \varepsilon \quad (5)$$

$$\%\mathrm{Ca}_{\mathrm{Nod}} = \frac{\alpha_{\mathrm{Nod}} \times [\mathrm{Ca}]_{\mathrm{Nod}} \times \rho_{\mathrm{Nod}}}{\alpha_{\mathrm{Res}} \times [\mathrm{Ca}]_{\mathrm{PM}} \times \rho_{\mathrm{PM}}} \times \varepsilon \quad (6)$$

$$\%\mathrm{Ca}_{\mathrm{Total}} = \%\mathrm{Ca}_{\mathrm{Nod}} + \%\mathrm{Ca}_{\mathrm{SCarb}} \quad (7)$$

where α is the volumetric fraction of the different kinds of palaeo-Vertisols (% of skeleton for carbonate nodules, % of carbonate in soil fine earth for micritic soil carbonate, and the missing fraction necessary to reach 100% is attributed to the residue), Ca is the Ca concentration, and ρ the density. Details of calculations are given in Supplementary Material SC, results and associated propagated error listed in Table 3.

Errors are up to 46% and mainly due to the variability in the skeletal content. As shown in Diaz et al. (2016a), the skeletal content is very heterogenous with depth. Calculations show that there is a slight enrichment of Ca (30%) in the residue of palaeo-Vertisols compared to the initial CRPM. If the error span is considered, the Ca content remains useful when comparing the palaeo-Vertisols and the CRPM. This slight enrichment can be due to the dissolution of carbonate, which can occur during the present-day, as the system is no longer in equilibrium with the environmental conditions. Indeed, the climate, and thus the soil moisture, are different in the present-day compared to the main period of carbonate nodule precipitation, which occurred by the end of the African Humid Period (Diaz et al., 2018). When considering the granite end member as the initial parent material, the residue of palaeo-Vertisols is strongly depleted in Ca (an 80% loss of Ca in the present-day palaeo-Vertisol residue compared to granite). The lost Ca fraction was displaced to the carbonate phases or/and was exported from the geosystem.

In contrast, carbonate phases of the palaeo-Vertisols are obviously extremely enriched in Ca, that is, an increase of 746% compared to the CRPM as parental material, meaning that, regarding Ca, more than seven volumetric units of CRPM are needed to produce one volumetric unit of carbonate phases in the palaeo-Vertisol. This large increase of Ca can be explained by lateral transfer as shown in Bocquier (1971). Even when calculations are performed based on granite as the parent material, a slight Ca enrichment still takes place (value >100%), clearly demonstrating that an additional source of Ca is necessary to explain the mass balance.

TABLE 3 Ca depletion/accumulation, considering the CRPM or the granite as parent materials with the associated propagated error, calculated using the standard error

	CRPM (initial)	Error (%)	Granite	Error (%)
Ca_{Res}	1.3 ± 0.3	21	0.2 ± 0.05	30
Ca_{SCarb}	2.1 ± 0.8	39	0.3 ± 0.1	44
Ca_{Nod}	5.4 ± 2.2	40	0.8 ± 0.4	46
Ca_{Total}	7.5 ± 2.7	36	1.1 ± 0.4	37

Ca_{Res} for Ca depletion/accumulation in the palaeo-Vertisol residue compared to the parent material; Ca_{SCarb}: for Ca depletion/accumulation in the soil carbonate compared to the parent material; Ca_{Nod} for Ca depletion/accumulation in the carbonate nodules compared to the parent material. Ca_{Total} is total Ca depletion/accumulation in the carbonate nodules and carbonate soil compared to the parent material.

Consequently, Vertisols with their associated carbonate nodules acted as a trapping compartment for Ca at the landscape scale. Calcium was not transferred into the rivers when the system was active, highlighting the potential impact of carbonate nodules in soils on river geochemistry. Today, some dissolution probably occurs as the system is no longer in equilibrium with the climate and the river geochemistry is probably impacted by this process. In other contexts (travertine in two silicate watersheds from Nepal and southern Tibet), Tipper et al. (2006) also reported that secondary carbonates have a significant influence on river geochemistry and further assessment of the river geochemistry would be necessary to confirm this hypothesis for the Far North of Cameroon.

5.2.2 | Impact of pedogenic carbonate and the concept of 'Geochemical cascade'

Pedogenic carbonate nodules impact the river geochemistry at two different stages: (a) during their precipitation, as a part of the Ca being released from the granite and sequestered in Vertisols as secondary carbonate, and (b) during secondary carbonate dissolution, when Ca, which does not originate from the present-day bedrock weathering, is exported to the rivers. In the first case, carbonate nodules act as a carbon sink, whereas in the second case, nodules constitute a buffer compartment regarding Ca. Carbon sequestration has already been observed in terrestrial carbonate environments and several studies have already suggested that it be recognised in the global carbon budget (Harrison & Dorn, 2014; Monger et al., 2015). This study pointed out that, obviously, calcium sequestration also occurs in terrestrial carbonate, as in the Far North of Cameroon, where Ca has been trapped in the carbonate nodules since 6 ka BP, impacting the calcium and carbon coupled continental cycle.

This consequence goes beyond the study site as carbonate nodules are not limited to the Far North of Cameroon. Vertisols with carbonate nodules in silicate watersheds are also reported in numerous and extensive areas along the Sudano-Sahelian belt, for example, in Senegal (Maignien, 1965), Benin (Viennot, 1978), Togo (Lamouroux, 1969), Chad (Bocquier & Audry, 1975; Chevery & Fromaget, 1970; Vizier & Fromaget, 1970), Niger (Bocquier et al., 1964), Burkina Faso (Pottier, 1973), Mali (Maignien, 1961) and Central African Republic (Boulvert, 1983). To a larger extent, Vertisols cover 309 million hectares worldwide, which represents 2% of the land cover (USDA-NRCS, 1999). In Mule Hole and Tamil Nadu areas (India), Vertisols with pedogenic carbonate (as nodules and/or calcrete) have also been observed in silicate watersheds (Durand et al., 2006; Violette et al., 2010a) and Violette et al. (2010b) demonstrated that 40% of the Ca exported from the watershed originated from pedogenic carbonate.

Consequently, secondary carbonate must not be discarded or neglected in chemical weathering calculations, as it undoubtedly has an impact on the global carbon budget. Indeed, elements do not travel directly from the substratum to the rivers through weathering, because some of them can be trapped in terrestrial secondary deposits for an undetermined time. For example, the fact that the palaeo-Vertisols from the Far North of Cameroon are presently undergoing erosion points to a future new transfer from a fossil and transient compartment of carbonate nodules to downstream systems. This dynamic vision of a transfer pathway from granite, to soil solution, then to nodules and finally to sediments and/or river waters downstream is a perfect geochemical illustration of the concept of 'sediment cascade' (Burt & Allison, 2010). Indeed, this concept introduced as 'the transfer of sediment and water from points of generation in upland environments, through transport pathways and intermediate stores to the coastal zone and oceanic sinks' (Burt & Allison, 2010) can equally be applied to the elements as a 'geochemical cascade' by simply replacing 'the transfer of sediment' by 'the transfer of elements': travelling from one transient compartment to another, recombining or released, they ultimately end up in the ocean.

6 | CONCLUSIONS

This study case conducted in the Far North of Cameroon provided a qualitative and quantitative example of the role of pedogenic carbonate in silicate watershed geochemistry. It showed that there is a lag between the release of Ca from a source to the transfer of Ca into a river system. The geochemical compositions of palaeo-Vertisols and their associated carbonate nodules allowed three main processes to be highlighted. These processes led to the transfer of Ca from a source, in this case the granite and dust, to a trapping compartment, in this case pedogenic carbonate nodules. The first process involved the weathering of a granitic bedrock, which produced a saprolite. The residual products were then mixed with Saharan dust to form the host sediment of the nodules (CRPM). The reworked granitic arena provided plagioclases, which represented a significant source of Ca. Calcium released during silicate weathering was transferred into the soil solution. The second process is related to clay minerals, products of weathering. These clays had mainly a 2:1 structure, allowing Ca and other cations to accumulate during Vertisol development. Weathering products, that is, clays and oxides, as well as vegetation and soil organic matter, have to be considered as transient compartments of Ca, an intermediate step between the source and the trapping compartment. At the end of the African Humid Period, drier climate conditions prevailed, enhancing the precipitation and preservation of pedogenic carbonate nodules. Calcium was then incorporated into the nodules and sequestered as such, until the present-day. Consequently, during the last 20,000 years, a significant amount of calcium was transferred from upstream granite to downstream nodules of pedogenic carbonate developed in Vertisols. Calculations demonstrated that Ca accumulated in these palaeo-Vertisols in the form of carbonate nodules, highlighting the role of Vertisols as traps of Ca. In the Far North region of Cameroon, significant quantities of calcium remain sequestrated in the soil system not yet transferred into rivers. Therefore, these results emphasise the significant role of Vertisols in terrestrial Ca balances, as they cover large areas on Earth. In addition, such a spatial relationship between sources and transient trapping compartments illustrates the new concept of 'geochemical cascade' similar, in terms of geochemistry, to the concept of 'sediment cascade' developed by continental sedimentologists.

ACKNOWLEDGEMENTS

The authors want to thank Pr. Benjamin Ngounou Ngatcha and his team for their help in the field. The LMI PICASS'EAU from the IRD and the members of Water and Environmental Sciences Laboratory at the University of Ngaoundéré provided their help for logistical and technical support during the fieldwork in 2013. Dr Alexey Ulianov (ISTE, University of Lausanne) performed ICP-MS analyses, Loic Liberati provided his help in the laboratory (carbonate dosage and CEC) and Charlotte Skonieczny in the estimatation of the geochemical composition of the Saharan dust. The authors would like to thank the two anonymous reviewers who substantially improved the first version of the manuscript. Karin Verrecchia edited the manuscript. This study has been supported by a Swiss National Science Foundation grant no. 200021-147038 to EPV and is part of the work carried out within the frame of the LMI DYCOFAC and the CALAKÉ project supported by the Labex OT-Med. Data are available on request to the authors.

ORCID

Fabienne Dietrich https://orcid.org/0000-0002-8239-3818
Pierre Deschamps https://orcid.org/0000-0003-1687-3765

REFERENCES

Abouchami, W., Näthe, K., Kumar, A., Galer, S.J., Jochum, K.P., Williams, E. et al. (2013) Geochemical and isotopic characterization of the Bodélé Depression dust source and implications for transatlantic dust transport to the Amazon Basin. *Earth and Planetary Science Letters*, *380*, 112–123.

Aide, M. & Smith-Aide, C. (2003) Assessing soil genesis by rare-earth elemental analysis. *Soil Science Society of America Journal*, *67*, 1470–1476.

Amaral, P.G.C., Vincens, A., Guiot, J., Buchet, G., Deschamps, P., Doumnang, J.C. et al. (2013) Palynological evidence for gradual

vegetation and climate changes during the African Humid Period termination at 13 degrees N from a Mega-Lake Chad sedimentary sequence. *Climate of the Past*, *9*(1), 223–241.

Arunchalam, J., Emons, H., Krasnodebska, B. & Mohl, C. (1996) Sequential extraction studies on homogenized forest soil samples. *The Science of the Total Environment*, *181*, 147–159.

Aubert, D., Stille, P. & Probst, A. (2001) REE fractionation during granite weathering and removal by waters and suspended loads: Sr and Nd isotopic evidence. *Geochimica et Cosmochimica Acta*, *65*, 387–406.

Begonha, A. & Braga, M.S. (2002) Weathering of the Oporto granite: Geotechnical and physical properties. *Catena*, *49*, 57–76.

Berner, R.A., Lasaga, A.C. & Garrels, R.M. (1983) The carbonate-silicate geochemical cycle and its effect on atmospheric carbon dioxide over the past 100 million years. *American Journal of Science*, *283*, 641–683.

Bickle, M.J., Tipper, E., Galy, A., Chapman, H. & Harris, N. (2015) On discrimination between carbonate and silicate inputs to Himalayan rivers. *American Journal of Science*, *315*(2), 120–166.

Bigham, J.M., Fitzpatrick, R.W., Schulze, D.G. & Dixon, J.B. (2002) Iron oxides. In: Dixon, J.B. & Schulze, D.G. (Eds.) *Soil mineralogy with environmental applications*. SSSA Book Series. Soil Science Society of America, pp. 323–366.

Blokhuis, W.A. (1993) Vertisols in the central clay plain of the Sudan. Thesis Wageningen, Agricultural University, Wageningen, pp. 1–323.

Bocquier, G. (1971) Genèse et évolution de deux toposéquences de sols tropicaux du Tchad: Interprétation biogéodynami que. *Cahier de ORSTOM, Série pédologie*, *9*, 510–515.

Bocquier, G. & Audry, F. (1975) Carte pédologique de reconnaissance de la République du Tchad à 1/200 000, Feuille Abou-Goulem, Adre, Am Zoer, Guereda. *ORTSTOM, Notice Explicative*, *61*, 115.

Bocquier, G., Gavaud, M., Boulet, R. & Alboucq, G. (1964) Carte pédologique de reconnaissance de la République Populaire du Niger 1/500000, Feuille Niamey-Zinder-Maradi. ORTSTOM.

Boulvert, Y. (1983) Carte pédologique de la République Centrafricaine à 1/1 000 000. *ORTSTOM, Notice Explicative*, *100*, 133.

Brabant, P. & Gavaud, M. (1985) Les sols et les ressources en terres du Nord-Cameroun. *ORTSTOM, Notice Explicative*, *103*, 369.

Braun, J.-J., Pagel, M., Muller, J.-P., Bilong, P., Michard, A. & Guillet, B. (1990) Cerium anomalies in lateritic profiles. *Geochimica et Cosmochimica Acta*, *54*, 781–795.

Braun, J.-J., Viers, J., Dupré, B., Polve, M., Ndam, J. & Muller, J.-P. (1998) Solid/liquid REE fractionation in the lateritic system of Goyoum, East Cameroon: The implication for the present dynamics of the soil covers of the humid tropical regions. *Geochimica et Cosmochimica Acta*, *62*, 273–299.

Bristow, C.S., Hudson-Edwards, K.A. & Chappell, A. (2020) Fertilizing the Amazon and equatorial Atlantic with West African dust. *Geophysical Research Letters*, *37*, L14807.

Burt, T. & Allison, R.J. (2010) *Sediment cascades: An integrated approach*. Chichester: John Wiley and Sons.

Cao, X., Chen, Y., Wang, X. & Deng, X. (2001) Effects of redox potential and pH value on the release of rare earth elements from soil. *Chemosphere*, *44*, 655–661.

Castillo, S., Moreno, T., Querol, X., Alastuey, A., Cuevas, E., Herrmann, L. et al. (2008) Trace element variation in size-fractionated African desert dusts. *Journal of Arid Environments*, *72*, 1034–1045.

Cerling, T.E. (1984) The stable isotopic composition of modern soil carbonate and its relationship to climate. *Earth and Planetary Science Letters*, *71*, 229–240.

Chevery, C. & Fromaget, M. (1970) Carte pédologique de reconnaissance de la République du Tchad à 1/200 000, Feuille de Léré. *ORTSTOM, Notice Explicative*, *40*, 93.

Ciesielski, H., Sterckeman, T., Santerne, M. & Willery, J.P. (1997) Determination of cation exchange capacity and exchangeable cations in soils by means of cobalt hexamine trichloride. Effects of experimental conditions. *Agronomie*, *17*, 1–7.

Clauer, N. & Paquet, H. (1997) *Soils and sediments. Mineralogy and Geochemistry*. Berlin: Springer.

Compton, J.S., White, R.A. & Smith, M. (2003) Rare earth element behavior in soils and salt pan sediments of a semi-arid granitic terrain in the Western Cape, South Africa. *Chemical Geology*, *201*, 239–255.

Coppin, F., Berger, G., Bauer, A., Castet, S. & Loubet, M. (2002) Sorption of lanthanides on smectite and kaolinite. *Chemical Geology*, *182*, 57–68.

Coulombe, C.E., Dixon, J.B., Wilding, L.P., Ahmad, N. & Mermut, A. (1996) Mineralogy and chemistry of vertisols. In: Ahmad, N. & Mermut, A. (Eds.) *Vertisols and technologies for their management*. Amsterdam: Elsevier sciences B.V., pp. 115–200.

Cramer, M.D. & Barger, N.N. (2014) Are mima-like mounds the consequence of long-term stability of vegetation spatial patterning? *Palaeogeography, Palaeoclimatology, Palaeoecology*, *409*, 72–83.

Da Silva, J.F. & Williams, R.J.P. (2001) *The biological chemistry of the elements: The inorganic chemistry of life*. Oxford: Oxford University Press.

de Menocal, P., Ortiz, J., Guilderson, T., Adkins, J., Sarnthein, M., Baker, L. et al. (2000) Abrupt onset and termination of the African humid period: Rapid climate responses to gradual insolation forcing. *Quaternary Science Reviews*, *19*, 347–361.

Diaz, N., Dietrich, F., Cailleau, G., Sebag, D., Ngatcha, B.N. & Verrecchia, E.P. (2016a) Can mima-like mounds be Vertisol relics (Far North Region of Cameroon, Chad Basin)? *Geomorphology*, *261*, 41–56.

Diaz, N., Dietrich, F., Sebag, D., King, G.E., Valla, P.G., Durand, A. et al. (2018) Pedo-sedimentary constituents as paleoenvironmental proxies in the Sudano-Sahelian belt during the Late Quaternary (southwestern Chad Basin). *Quaternary Science Reviews*, *191*, 348–362.

Diaz, N., King, G.E., Valla, P.G., Herman, F. & Verrecchia, E.P. (2016b) Pedogenic carbonate nodules as soil time archives: Challenges and investigations related to OSL dating. *Quaternary Geochronology*, *36*, 120–133.

Dietrich, F., Diaz, N., Deschamps, P., Ngatcha, B.N., Sebag, D. & Verrecchia, E.P. (2017) Origin of calcium in pedogenic carbonate nodules from silicate watersheds in the Far North Region of Cameroon: Respective contribution of in situ weathering source and dust input. *Chemical Geology*, *460*, 54–69.

Dincher, M., Calvaruso, C. & Turpault, M.-P. (2020) Major element residence times in humus from a beech forest: The role of element forms and recycling. *Soil Biology and Biochemistry*, *141*, 107674.

Dohrmann, R. & Kaufhold, S. (2009) Three new, quick CEC methods for determining the amounts of exchangeable calcium cations in calcareous clays. *Clays and Clay Minerals*, *57*, 338–352.

Durand, N., Ahmad, S.M., Hamelin, B., Gunnell, Y. & Curmi, P. (2006) Origin of Ca in South Indian calcretes developed on metamorphic rocks. *Journal of Geochemical Exploration*, *88*, 275–278.

Egli, M. & Fitze, P. (2000) Formulation of pedologic mass balance based on immobile elements: A revision. *Soil Science*, *165*, 437–443.

Eswaran, H. & Bin, W.C. (1978) A study of a deep weathering profile on granite in peninsular Malaysia: I. Physico-chemical and micromorphological properties. *Soil Science Society of America Journal*, *42*, 144–149.

Eswaran, H., Reich, P.F., Kimble, J.M., Beinroth, F.H., Padmanabhan, E. & Moncharoen, P. (2000) Global carbon stocks. In: *Global climate change and pedogenic carbonates*. Lewis Publishers, pp. 15–25.

Evans, C.V. & Bothner, W.A. (1993) Genesis of altered Conway granite (grus) in New Hampshire, USA. *Geoderma*, *58*, 201–218.

Fedo, C.M., Nesbitt, H.W. & Young, G.M. (1995) Unraveling the effects of potassium metasomatism in sedimentary rocks and paleosols, with implications for paleoweathering conditions and provenance. *Geology*, *23*, 921–924.

Gaillardet, J., Dupré, B., Louvat, P. & Allegre, C.J. (1999) Global silicate weathering and CO_2 consumption rates deduced from the chemistry of large rivers. *Chemical Geology*, *159*, 3–30.

Garcin, Y., Deschamps, P., Ménot, G., De Saulieu, G., Schefuß, E., Sebag, D. et al. (2018) Early anthropogenic impact on Western Central African rainforests 2,600 y ago. *Proceedings of the National Academy of Sciences of the United States of America*, *115*(13), 3261–3266.

Garrels, R.M. & Mackenzie, F.T. (1971) *Evolution of sedimentary rocks*. New York: Norton.

Gazel, J., Guiraudie, C., de Ribes, G.C., Cirotteau, A. & Leroy, B. (1956) Carte géologique du Cameroun. Direction des mines et de la geologie du Cameroun.

Gross, A., Palchan, D., Krom, M.D. & Angert, A. (2016) Elemental and isotopic composition of surface soils from key Saharan dust sources. *Chemical Geology*, *442*, 54–61.

Harrison, E.J. & Dorn, R. (2014) Introducing a terrestrial carbon pool in warm desert bedrock mountains, southwestern USA. *Global Biogeochemical Cycle*, *28*, 253–258.

Hasinger, O., Spangenberg, J.E., Millière, L., Bindschedler, S., Cailleau, G. & Verrecchia, E.P. (2015) Carbon dioxide in scree slope deposits: A pathway from atmosphere to pedogenic carbonate. *Geoderma*, *247*, 129–139.

Hervieu, J. (1967) Sur l'existence de deux cycles climato-sédimentaires quaternaires dans les monts Mandara et leurs abords (Nord-Cameroun). Conséquences morphologiques et pédogénétiques. *Comptes Rendus de l'Académie des Sciences, Paris*, *264*, 2624–2627.

Holland, H.D. (1984) *The chemical evolution of the atmosphere and oceans*. Princeton, NJ: Princeton University Press.

Huang, C. & Wang, C. (2004) Geochemical characteristics and behaviors of rare earth elements in process of Vertisol development. *Journal of Rare Earths*, *22*, 552–557.

Jacobson, A.D., Blum, J.D. & Walter, L.M. (2002) Reconciling the elemental and Sr isotope composition of Himalayan weathering fluxes: Insights from the carbonate geochemistry of stream waters. *Geochimica et Cosmochimica Acta*, *66*(19), 3417–3429.

Kabata-Pendias, A. & Pendias, H. (2011) *Trace elements in soils and plants*. Boca Raton, FL: CRC Press.

Kalu, A.E. (1979) The African dust plume: Its characteristics and propagation across West Africa in winter. *Scope*, *14*, 95–118.

Kovda, I., Mora, C.I. & Wilding, L.P. (2006) Stable isotope compositions of pedogenic carbonates and soil organic matter in a temperate climate Vertisol with gilgai, southern Russia. *Geoderma*, *136*, 423–435.

Kutílek, M., Ahmad, N. & Mermut, A. (1996) Water relations and water management of Vertisols. In: Ahmad, N. & Mermut, A. (Eds.) *Vertisols and technologies for their management*. Amsterdam: Elsevier sciences B.V., pp. 201–230.

Lal, R., Kimble, J.M., Stewart, B.A. & Eswaran, H. (2000) *Global climate change and pedogenic carbonates*, Lewis Publishers, 305 pp.

Lamotte, M., Bruand, A., Humbel, F.X., Herbillon, A.J. & Rieu, M. (1997) A hard sandy-loam soil from semi-arid northern Cameroon. 1. Fabric of the groundmass. *European Journal of Soil Science*, *48*, 213–225.

Lamouroux, M. (1969) Carte pédologique du Togo au 1/1000000. ORSTOM, Notice Explicative 34, 99 pp.

Laveuf, C. & Cornu, S. (2009) A review on the potentiality of rare earth elements to trace pedogenetic processes. *Geoderma*, *154*, 1–12.

Maignien, R. (1961) Etude des différentes vallées et plaines de la République du Mali. ORSTOM, 242 pp.

Maignien, R. (1965) Carte pedologique du Senegal au 1/1000.000. ORTSTOM, notice explicative, 71 pp.

Maley, J. (1981) Etudes Paylnologiques dans le Bassin du Tchad et Paléoclimatologie de l'Afrique Nord-Tropicale de 30000 ans à l'Epoque Actuelle. *Paleoecology of Africa*, *13*, 45–52.

Marcelino, V., Schaefer, C.E.G.R. & Stoops, G. (2018) Oxic and related materials. In: Stoops, G., Marcelino, V. and Mees, F. (Eds.) *Interpretation of micromorphological features of soils and regoliths*. Amsterdam, Netherlands: Elsevier, pp. 663–689.

Martin, D. (1961) *Carte pédologique du Nord-Cameroun au 1/100000e feuille Mora*. Yaoundé, Cameroun: ORSTOM-IRCAM.

Mermut, A.R., Padmanabham, E., Eswaran, H., Dasog, G.S., Ahmad, N. & Mermut, A. (1996) Pedogenesis. In: Ahmad, N. & Mermut, A. (Eds.) *Vertisols and technologies for their management*. Amsterdam: Elsevier sciences B.V., pp. 43–61.

Meybeck, M. (1987) Global chemical weathering of surficial rocks estimated from river dissolved loads. *American Journal of Science*, *287*, 401–428.

Migoń, P. & Thomas, M.F. (2002) Grus weathering mantles—Problems of interpretation. *Catena*, *49*, 5–24.

Mongelli, G. (1997) Ce-anomalies in the textural components of Upper Cretaceous karst bauxites from the Apulian carbonate platform (southern Italy). *Chemical Geology*, *140*, 69–79.

Monger, H.C., Kraimer, R.A., Cole, D.R., Wang, X. & Wang, J. (2015) Sequestration of inorganic carbon in soil and groundwater. *Geology*, *43*, 375–378.

Moreno, T., Querol, X., Castillo, S., Alastuey, A., Cuevas, E., Herrmann, L. et al. (2006) Geochemical variations in Aeolian mineral particles from the Sahara-Sahel Dust Corridor. *Chemosphere*, *65*, 261–270.

Morin, S. (2000) Géomorphologie. In: C. Seignobos (Ed.), *Atlas de la Province Extrême-Nord Cameroun. Ministère de la Recherche Scientifique et Technique*. Cameroun, Paris: Institut National de Cartographie, Institut de Recherche pour le Développement, 49 pp.

Négrel, P., Allègre, C.J., Dupré, B. & Lewin, E. (1993) Erosion sources determined by inversion of major and trace element ratios and strontium isotopic ratios in river water: The Congo Basin case. *Earth and Planetary Science Letters*, *120*, 59–76.

Nesbitt, H.W. & Markovics, G. (1997) Weathering of granodioritic crust, long-term storage of elements in weathering profiles, and petrogenesis of siliciclastic sediments. *Geochimica et Cosmochimica Acta*, *61*, 1653–1670.

Nesbitt, H.W. & Young, G.M. (1984) Prediction of some weathering trends of plutonic and volcanic rocks based on thermodynamic and kinetic considerations. *Geochimica et Cosmochimica Acta*, *48*, 1523–1534.

Nickel, E. (1973) Experimental dissolution of light and heavy minerals in comparison with weathering and intrastratal solution. *Contributions to Sedimentology*, *1*, 1–68.

Öhlander, B., Land, M., Ingri, J. & Widerlund, A. (1996) Mobility of rare earth elements during weathering of till in northern Sweden. *Applied Geochemistry*, *11*, 93–99.

Olivry, J.C. & Naah, E. (1999) Hydrologie. In: *Atlas de la Province Extrême-Nord Cameroun - Planche 3*, vol. 3. IRD Editions: Paris, pp. 1–32.

Peltier, R. (1993) In: *Les terres Hardé: Caracterisation et rehabilitation dans le bassin du lac Tchad*. Montpellier: CIRAD-Forêt, Cahiers Scientifiques, pp. 1–125.

Pottier, J.-C. (1973) Carte pédologique de reconnaissance de la République de Haute-Volta 1/500000, Ouest-Nord et Ouest-Sud. ORTSTOM.

Pourret, O., Davranche, M., Gruau, G. & Dia, A. (2007) Competition between humic acid and carbonates for rare earth elements complexation. *Journal of Colloid and Interface Science*, *305*, 25–31.

Pye, K. (1987) *Aeolian dust and dust deposits*. London: Academic Press Inc.

Rowley, M.C., Grand, S. & Verrecchia, É.P. (2018) Calcium-mediated stabilisation of soil organic carbon. *Biogeochemistry*, *137*, 27–49.

Rudnick, R.L. & Gao, S. (2003) In: *Composition of the continental crust*. Amsterdam: Elsevier, pp. 1-70.

Sako, A., Mills, A.J. & Roychoudhury, A.N. (2009) Rare earth and trace element geochemistry of termite mounds in central and northeastern Namibia: Mechanisms for micro-nutrient accumulation. *Geoderma*, *153*, 217–230.

Schaetzl, R.J. & Thompson, M.L. (2015) *Soils*. Cambridge: Cambridge University Press.

Scheuvens, D., Schütz, L., Kandler, K., Ebert, M. & Weinbruch, S. (2013) Bulk composition of northern African dust and its source sediments—A compilation. *Earth-Science Reviews*, *116*, 170–194.

Schlesinger, W.H. (1985) The formation of caliche in soils of the Mojave Desert, California. *Geochimica et Cosmochimica Acta*, *49*, 57–66.

Schlesinger, W. H. & Bernhardt, E. S. (2013) *Biogeochemistry: An analysis of global change*, 3rd edition, Academic Press, pp. 15–48.

Schwertmann, U. & Taylor, R.M. (1989) Iron oxides. In: Dixon, J.B. and Weed, S.B. (Eds.) *Minerals in soil environments*. Madison, WI: Soil Science Society of America, pp. 379–438.

Shanahan, T.M., McKay, N.P., Hughen, K.A., Overpeck, J.T., Otto-Bliesner, B., Heil, C.W. et al. (2015) The time-transgressive termination of the African Humid Period. *Nature Geoscience*, *8*, 140–144.

Sieffermann, G. (1967) Variations Climatiques au Quaternaire dans le Sud-Ouest de la Cuvette Tchadienne. Fonds Documentaires ORSTOM, 141, 12 pp.

Skonieczny, C., Bory, A., Bout-Roumazeilles, V., Abouchami, W., Galer, S.J.G., Crosta, X. et al. (2001) The 7–13 March 2006 major Saharan outbreak: Multiproxy characterization of mineral dust deposited on the West African margin. *Journal of Geophysical Research*, *116*, D18210.

Southard, R.J., Driese, S.G. & Nordt, L.C. (2011) Vertisols. In: *Handbook of soil science: Properties and processes*, 2nd edition. Boca Raton, FL: CRC Press, pp. 82–97.

Stiles, C.A., Mora, C.I. & Driese, S.G. (2003) Pedogenic processes and domain boundaries in a Vertisol climosequence: Evidence from titanium and zirconium distribution and morphology. *Geoderma*, *116*, 279–299.

Stoops, G. (2003) *Guidelines for analysis and description of soil and regolith thin sections*. Madison, WI: Soil Science Society of America Inc.

Suchel, J.-B. (1988) *Les climats du Cameroon*. France: Université de St-Etienne.

Tipper, E., Galy, A. & Bickle, M. (2006) Riverine evidence for a fractionated reservoir of Ca and Mg on the continents: Implications for the oceanic Ca cycle. *Earth and Planetary Science Letters*, *247*, 267–279.

Tipper, E.T., Schmitt, A.-D. & Gussone, N. (2016) Global Ca cycles: Coupling of continental and oceanic processes. In: *Calcium stable isotope geochemistry*. Berlin: Springer, pp. 173–222.

Turpault, M.P., Calvaruso, C., Dincher, M., Mohammed, G., Didier, S., Redon, P.-O. et al. (2019) Contribution of carbonates and oxalates to the calcium cycle in three beech temperate forest ecosystems with contrasting soil calcium availability. *Biogeochemistry*, *146*, 51–70.

Urey, H.C. (1952) *The planets: Their origin and development*. London: Mrs. Hepsa Ely Silliman Memorial Lectures, Yale University.

USDA-NRCS. (1999) *Titre Soil Taxonomy: A Basic System of Soil Classification for Making and Interpreting Soil Surveys*. 2nd edition, Numéro 436 de Agriculture handbook, United States: Division of Soil Survey, États-Unis. Natural Resources Conservation Service, U.S. Department of Agriculture, Natural Resources Conservation Service, Longueur 869 pp.

Verrecchia, E.P. (2011) Pedogenic carbonates. *Encyclopedia of geobiology*, pp. 721–725.

Viennot, M. (1978) Carte pédologique de reconnaissance de la République Populaire du Benin 1/200000, Feuille Kandi-Krarimama. ORTSTOM, Notice Explicative 66, 55 pp.

Violette, A., Godderis, Y., Maréchal, J.-C., Riotte, J., Oliva, P., Kumar, M.M. et al. (2010b) Modelling the chemical weathering fluxes at the watershed scale in the Tropics (Mule Hole, South India): Relative contribution of the smectite/kaolinite assemblage versus primary minerals. *Chemical Geology*, *277*, 42–60.

Violette, A., Riotte, J., Braun, J.J., Oliva, P., Marechal, J.C., Sekhar, M. et al. (2010a) Formation and preservation of pedogenic carbonates in South India, links with paleo-monsoon and pedological conditions: Clues from Sr isotopes, U-Th series and REEs. *Geochimica et Cosmochimica Acta*, *74*, 7059–7085.

Vizier, J.-F. & Fromaget, M. (1970) Carte pédologique de reconnaissance de la République du Tchad à 1/200 000, Feuille de Fainga et Lai. ORTSTOM, Notice Explicative, 39, 95 pp.

Walker, J.C., Hays, P.B. & Kasting, J.F. (1981) A negative feedback mechanism for the long-term stabilization of Earth's surface temperature. *Journal of Geophysical Research: Oceans*, *86*, 9776–9782.

Wieder, M. & Yaalon, D.H. (1982) Micromorphological fabrics and developmental stages of carbonate nobular forms related to soil characteristics. *Geoderma*, *28*, 203–220.

Zamanian, K., Pustovoytov, K. & Kuzyakov, Y. (2016) Pedogenic carbonates: Forms and formation processes. *Earth-Science Reviews*, *157*, 1–17.

SUPPORTING INFORMATION

Additional supporting information may be found online in the Supporting Information section.

How to cite this article: Dietrich F, Diaz N, Deschamps P, Sebag D, Verrecchia EP. Calcium transfer and mass balance associated with soil carbonate in a semi-arid silicate watershed (North Cameroon): An overlooked geochemical cascade? *Depositional Rec*. 2021;00:1–18. https://doi.org/10.1002/dep2.134